Original scientific paper

NUMERICAL SIMULATION OF SINGLE POINT INCREMENTAL FORMING FOR ASYMMETRIC PARTS

George-Christopher Vosniakos, Gabriel Pipinis, Protesilaos Kostazos

National Technical University of Athens, School of Mechanical Engineering,
Manufacturing Technology Laboratory, Athens, Greece

Abstract. *Single point incremental forming (SPIF) that will produce non-symmetric sheet metal parts has been rarely dealt with so far. SPIF of a Francis hydro-turbine vane made of aluminum alloy is studied as a typical example in this work. At first, a concave geometry, encompassing the desired vane shape is designed, from which the formed part will ultimately be cut out. The necessary SPIF toolpaths are created by using the CAM software normally used for milling processes. Based on these toolpaths, a finite element simulation is setup using shell elements with a particular emphasis on substantial time scaling and due care on tool-sheet contact parameters. For validation purposes the part was manufactured and digitized by a white light scanner. It exhibited tolerable deviation from the targeted nominal geometry. Simulation predicted a significant part of this deviation, proving its indispensability in checking out toolpaths and process parameters for non-symmetric parts, yet at non-negligible computational time.*

Key words: *Single Point Incremental Sheet Forming, Non-symmetry, Toolpath, Finite Elements, Time Scaling*

1. INTRODUCTION

The single point incremental forming (SPIF) process for sheet metal parts does not require a die but only a blank holding fixture and a simple forming tool to operate on a computer numerically controlled (cnc) milling machine. Therefore, it is suited to small batch manufacturing and prototyping [1].

SPIF process is associated with better formability compared to conventional forming processes. The exact reason for this as well as the principal forming mechanism seems to be unclear. The latter has been related to the stretching of the sheet, which has a lot in common with conventional drawing; this has been adopted by many researchers, due to

its simplicity. The area in which yielding manifests itself is small and it is constantly changing; thus neck formation is suppressed leading to enhanced formability [1]. On the contrary, many researchers have acknowledged the importance of thru thickness shear [2] and bending [3] in the 'radial' direction. The isotropic stress also seems to have an important role in the forming process [4]. As a result, the use of fracture forming limit (FFL) is recommended [2].

SPIF tools are usually made of tool steels or carbides and are classified according to end shape: round-ball, which is the most common one, cylindrical and roller-ball. The rolling ball seems to benefit surface quality and formability due to reduction of friction, but it is more complicated to produce and limits the maximum sheet-wall angle so that contact of the sheet is only made to the rolling ball [5].

Tool size has been mostly studied for round-end tools. In principle, a tool with a smaller radius has a positive effect in formability [6]. However, it has been also pointed out [7] that as the tool radius gets smaller a "squeezed-out wall" defect appears in the surface. Step down and material properties also contribute to the presence and intensity of this defect. Thus, tool selection should be based on tool size to sheet thickness ratio [8]. Formability is also related to the maximum achievable wall angle [9].

The toolpath most often starts from the edge of the cavity that is to be constructed and ends at its bottom. When multiple trajectories are used, some of them may start from the bottom of the cavity. Indeed, multiple trajectories can lead to substantial increase in formability [10].

Feed speed and the step down speed may be constant so as to create a helical toolpath. Discrete step down have also been used to create a "Z-level" toolpath, but the helical toolpath results in more even strain distribution [11]. Step down (and stepdown speed for helical toolpaths) is selected in dependence of the other process parameters and it heavily influences surface quality as well as formability of the part [3]. Spindle speed is selected so as to achieve favorable friction conditions. For tools with a round-end one of the following two seemingly contradictory strategies is used: (a) minimizing the average sliding speed in the contact area between the part and tool (b) increasing the temperature in the contact area due to a high relative speed between the sheet and the tool, thus increasing formability. The optimum spindle speed varies in dependence of the rest of the process parameters [12].

For the manufacture of some complex parts a "featured based trajectory" has been proposed. The toolpath has a constantly variable stepdown speed as to adapt to the distinct features of the part shape (e.g. bottom edges with variable depth) [13].

In the overwhelming majority of SPIF applications reported in literature axisymmetric parts have been processed. However, lack of symmetry is most interesting since it constitutes the general case of engineering part shapes encountered. This work is devoted to exploring SPIF of non-symmetric parts by example of a Francis hydro-turbine vane, aiming to point out the use of numerical modeling and simulation in such cases. Section 2 reviews numerical modeling techniques pertaining to SPIF. Section 3 presents the case study. Section 4 outlines simulation setup and Section 5 the results obtained. Section 6 describes the validation experiment. A discussion of results is provided in Section 7. The conclusions drawn are summarized in Section 8.

2. LITERATURE REVIEW ON FINITE ELEMENT ANALYSIS OF SPIF

The explicit FEA method seems to be preferred in forming process simulations, including the SPIF case because it is faster [14,15], even though the implicit method may lead to better accuracy [16]. There is a limitation in the maximum time step (Courant time step). To further decrease the time step two methods can be implemented: time scaling and mass scaling. These methods may cause a significant (artificial) increase in the total kinematic energy, with a negative effect in the overall accuracy of the results. Note that in SPIF the total kinematic energy is typically a small fraction of the total energy [17].

Solid elements may be thought to represent the sheet in a more accurate way than shell elements. However, many issues arise if there is no sufficient through-thickness discretization, typically less than 4 elements: shear locking, hourglass modes, poor nonlinear bending. Such issues are dealt with at the expense of computational time [18] or by novel element types [19]. A 3D shell, the solid-shell element, offers a better representation of the problem, and can resolve solid-element issues. It has been also used in SPIF simulations for high accuracy. However, this still needs usually 2-3 through thickness elements; it seems to fail in patch tests and it has limited adaptive re-meshing capability [20]. Shell elements, despite their being 3D, can successfully deal with bending, through thickness shear, stretching normal to the surface and others with suitable formulation [18]. They are faster than solid and solid-shell elements and they achieve very good results in forming processes if they are used with 5 to 9 through thickness integration points. The latter are necessary for simulating plastic bending [21, 22]. A better compromise between accuracy and computation time in many cases including SPIF [14] is struck by adaptive re-meshing in areas with significant concavity or stress gradient, e.g. near the SPIF tool. However, adaptive re-meshing is neither standard nor robust in most FEA programs [21].

As far as boundary conditions are concerned, fixed end support was applied in the area where the sheet is clamped. However, very small, in-plane translation of the fixed nodes, due to elasticity or slippage, may heavily influence the results of the simulation [23]. As far as material property modeling is concerned, the use of an anisotropic yield criterion, such as Hill's, is important, especially for cold rolled sheets [21]. In-plane anisotropy can be assumed. Thus, the yield locus is calculated based on the yield stress and Lankford coefficient (usually R0 ,R45,R90) that are easily determined [24, 25].

The exponential hardening law (swift power law) is a popular choice for the simulation of many materials [3, 21]. The mixed work-kinematic model takes into consideration the Bauschinger effect as well, which seems to have a substantial impact in SPIF process [26]. However, the mixed model is based on two parameters that are difficult to be determined as they are strain dependent.

Recent literature summarizes finite element modeling issues as mentioned above and suggests possible solutions [27].

3. PART AND TOOLPATH GEOMETRY

The part to be manufactured is a Francis hydro-turbine vane with a 132 mm chord length, see Fig. 1(a). The part was manufactured from AA6082O annealed according to the material provider's recommendations (Leichtmetall). Manufacturing of a cavity (cup-shape) starting from a flat sheet is necessary from which the vane will be finally cut-out, e.g. by laser. The cavity was created in a 3D CAD environment, starting from the vane's convex surface

geometry, i.e. neglecting its varying thickness and taking into account the following considerations: (a) the wall angle has to be restricted so as to minimize the probability of fracture during SPIF. Of particular importance was the cavity area near the vane in order to avoid thinning of the formed part (b) Geometry of the cavity corresponding to the roughing phase was modified so as to minimize curvature and avoid features that could increase dimensional deviation (c) Size of the flat sheet was restricted so as to reduce manufacturing time and cost (d) The vane had to be positioned at a sufficient distance away from the edge of the cavity, where excessive dimensional deviation is expected. Spring-back was not taken into consideration when designing the cavity.
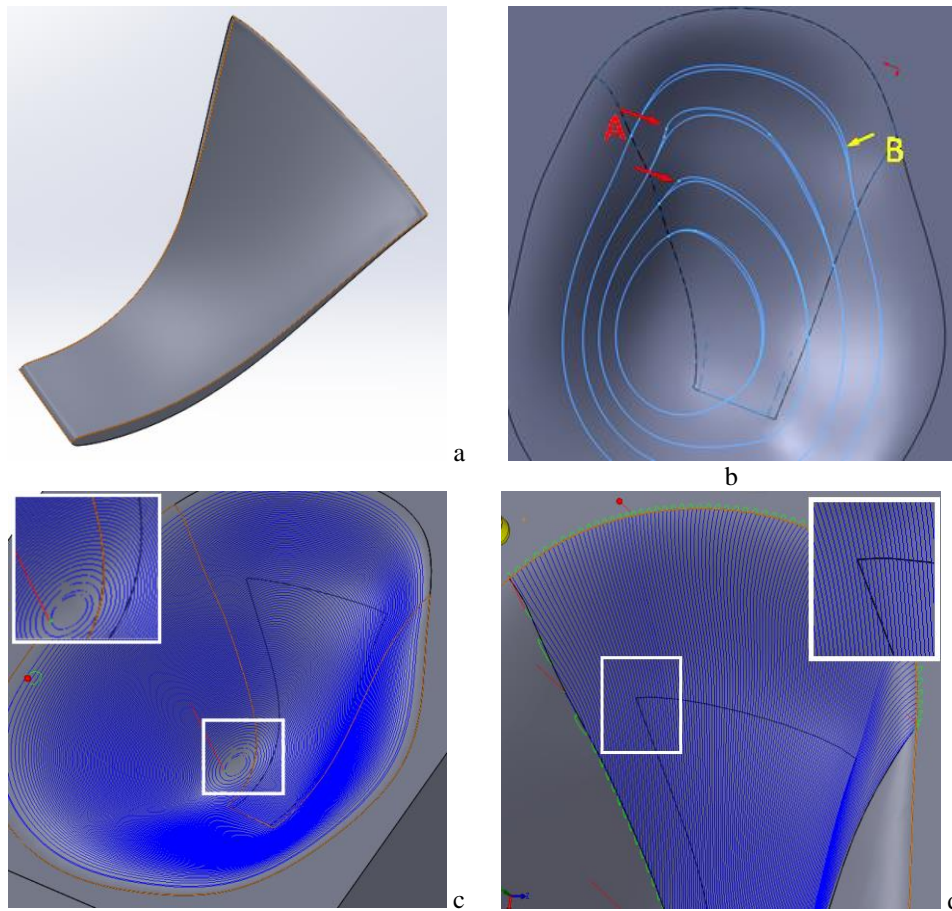
Fig. 1 (a) Vane ideal shape (b) cavity contour lines for roughing (A) and finishing (B) passes (c) helical toolpath for roughing (d) zigzag toolpath for finishing

Two toolpaths corresponding to roughing and finishing were created using SolidCAM™. Sample contours corresponding to the roughing and finishing cavity shape that was considered as a guide for constructing the toolpaths are compared in Fig. 1(b). Roughing was assigned a helical toolpath and finishing was assigned a zig-zag toolpath see Fig. 1(c-d). The

parameters used in both phases were consistent with literature recommendations for each material used. A round ball-end tool with diameter 7 mm was chosen for formability and surface quality [28]. Spindle speed was 50 rpm in order to keep relative speed between the sheet and the tool at low levels. Feed was set to F=1000 mm/min and stepdown was set to D=0.445mm for formability and surface quality [28].

4. NUMERICAL SIMULATION MODEL SETUP

To simulate SPIF for the non-symmetric cavity presented above, the Finite Element software LS Dyna R8.1 was employed with the default explicit integration method. The main issues regarding model setup are presented next.

4.1. Meshing and re-meshing

The mesh consists of two parts, the sheet (slave surface) and the tool (master surface). The tool was simulated with a hollow sphere meshed with hexa elements. The sheet was assumed as a surface discretized mainly by square shell elements (Belytscko-Tsay) with five through-thickness integration nodes. This element formulation offered sufficient accuracy with high robustness and low computational cost.

Re-meshing and fusion were based on the total angle change relative to the surrounding elements in order to fulfill three criteria, namely to: (a) sufficiently represent the sheet curvature, especially at the edge of the cavity bottom (cup) (b) minimize the number of elements, especially in areas with minor interest in the simulation, and (c) keep contact constant between the remeshed elements and the tool. Note that contact between the original mesh and the tool may cause sudden re-meshing and excessive strains in the contact area. A very aggressive fusion strategy seems to also cause stability issues.

The value of the angle based on which re-meshing takes place has to be reset three times in order to satisfy the above requirements. This was necessary in order to fulfill the third criterion in the beginning of the process, where the angles and the deformations were relatively small. Resetting the value in fusion was unexpectedly not possible, reducing the positive impact of the whole re-meshing-fusion algorithm.

Areas near the fixed support were initially remeshed and excluded from adaptive re-meshing for two reasons: (a) deformation in these areas was significant making a fine mesh important (b) adaptive re-meshing causes a sudden change in geometry leading to oscillation of the sheet.

4.2. Tool-sheet contact

A penalty based segment to segment search algorithm was utilized. Node forces are calculated based on the distance among surfaces or edges instead of the classic node-surface distance. Although computationally more demanding, this method was selected as contact simulation was a particularly challenging task. In particular, the number of elements in contact was low. In addition, the size of the master elements had to be optimized in order to minimize the impact of the acute edges and vertices in the master surface, and the poor master/slave element size ratio. Therefore, discretization problems were caused as well as noise in the contact. Thus, the segment to segment algorithm led to a more gradual transition of the contact between neighboring elements.

4.3. Material model

The yield locus was calculated by the Barlat's Yld2000 model, drawing on the equivalent shear yield energy. It captures a plane anisotropic behavior and depends on initial yield strength and Lankford coefficients in the 0º, 45º, 90º directions with respect to rolling direction. The parameters needed for the stress-strain model and the yield locus were defined from tensile tests according to E8_m and E517_m ASTM International standards performed on an Instron™ model 4482 testing machine. The 'dogbone' specimens were created by CNC milling using mild cutting conditions and cutting fluid. The rest of the parameters were adopted from the respective alloy manufacturers (Leichtmetall). Hardness was assessed by a Vickers hardness tester. Material parameter values are shown in Table 1. Analysis (regression-extrapolation) of the tensile test concluded that stress-strain dependence was best represented by the exponential model.

Table 1 AA6082O properties used

Property	Value
Density (gr/mm3)	0.0027
Young Modulus (GP)	69
Poisson ratio	0.33
Yield Strength (MPa)	83.5
Strength Coefficient -k (MPa)	242
Strain Hardening –n	0.21
Hardness (HV)	76
Elongation at break	0.18

4.4. Boundary conditions

Sheet clamping was simulated as fixed support. 3D rigid body motion is imposed on the spherical tool, according to the G-code created during toolpath generation stage, see Section 3, and a time-displacement file resulting from G-code processing by a Matlab custom-written script. The feeding speed of the tool was increased by 300 times compared to the actual speed (time scaling). The spindle speed was neglected.

4.5. Stability enhancement

Due to the reduced integration formulation of the Belytchko Tsay elements, kinematic hourglass control had to be used. In addition, damping was implemented in the nodes, especially in the contact area, to reduce the impact of time scaling. Selective mass scaling was used in some elements near the fixture because they possessed shorter edges.

5. SIMULATION RESULTS

After termination of the SPIF simulation, a spring-back simulation was carried out using an implicit integration method. During this stage, the sheet was set free from the boundary conditions and the final sheet shape was obtained as a 3D solid body.

A full simulation run lasts about 290 hours on a 6-core AMD Ryzer 7 CPU memory being of lesser importance.

5.1. Plastic strain and thinning

Thinning estimation is very important for the prediction of fracture-cracking. No excessive thinning was observed in the simulated case. At the 2nd stage of the process (zig-zag toolpath), a small increment in strain appears, see Fig. 2, albeit much less confined to the tool contact zone in comparison to deformation at the 1st stage (helical toolpath). Strain magnitude as well as thinning, see Figs. 2 and 3, are correlated to the wall angle.
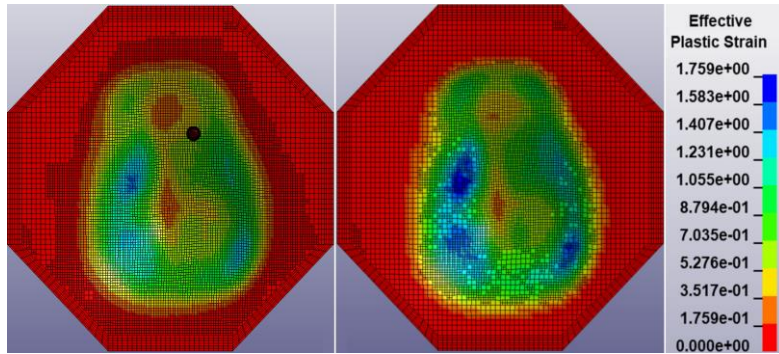

Fig. 2 Simulated effective plastic strain after 1st stage (left) and 2nd stage (right)
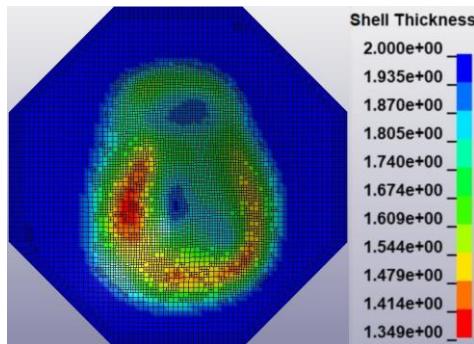
Fig. 3 Simulated shell thickness distribution

5.2. Force on the tool

SPIF force can be broken down into three components: one along the tool axis (Z direction), constituting the axial component, which is the largest, and two on the horizontal plane (X and Y directions) constituting the radial component. Fig. 4(a) and (b) depicts the variation of these forces for the roughing and finishing phases, respectively. The maximum axial force reached 1750 N whilst maximum radial force reached 700 N. Note that equivalent tensile yield stress was calculated at 200 MPa, the average equivalent strain acquiring a value of about 0.45.

a)

b)
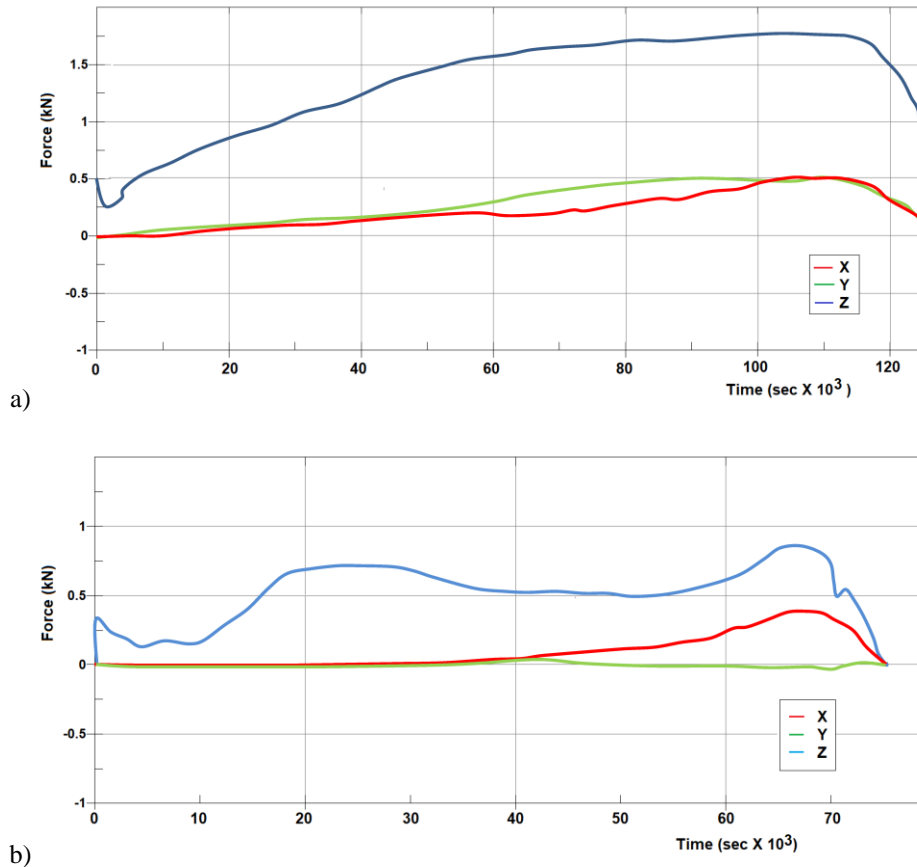
Fig. 4 Tool force envelope (a) Helical roughing toolpath (b) zig-zag finishing toolpath

During SPIF with a helical toolpath, see Fig. 1(c), the force constantly increases in the first half of the process duration. This is due to the material hardening and the lower wall angle. Then, the force remains stable for most of the second half of the process duration, whilst at the end it decreases due to the lower wall angles locally. The variation pattern for the finishing phase is different, forces hardly reaching half the magnitude of the roughing phase, see Fig. 4(b).

6. EXPERIMENTAL VALIDATION

6.1. Fixture and tool

The blank holding fixture was designed on Solidworks[TM] and tested for strength and deformation on ANSYS[TM] employing the worst-case forces that resulted from SPIF simulation. The required clamping force was calculated on ANSYS, taking in consideration the cyclic nature of SPIF loading, resulting in total necessary pre-tension of 400 kN

distributed over 20 M12 bolts. Maximum deformation of the fixture resulted to 0.17 mm and was deemed acceptable, see Fig. 5.
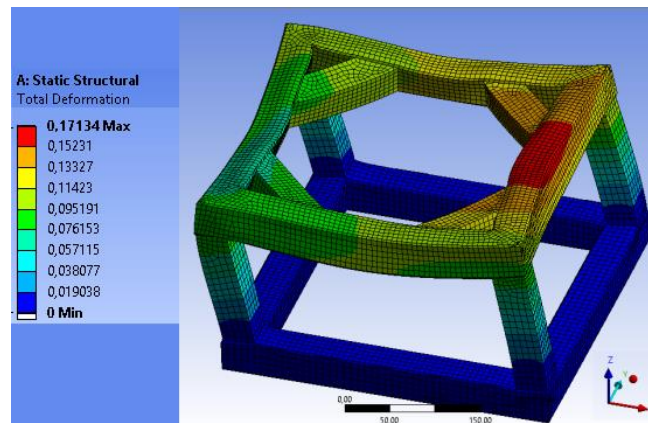
Fig. 5 Deformation of the work-holding fixture

The fixture was manufactured from arc welded square steel tubes (40x40mm cross-section and 2mm wall thickness), see Fig. 6(a). A ball-end tool with a radius of 7 mm was employed, see Fig. 6(b). It was manufactured from stainless steel (304L) on a HAAS TL-1 CNC lathe. Its hardness was measured at 270 HV30, which was deemed sufficient for SPIFing of aluminum, whose hardness was 36 HV30.
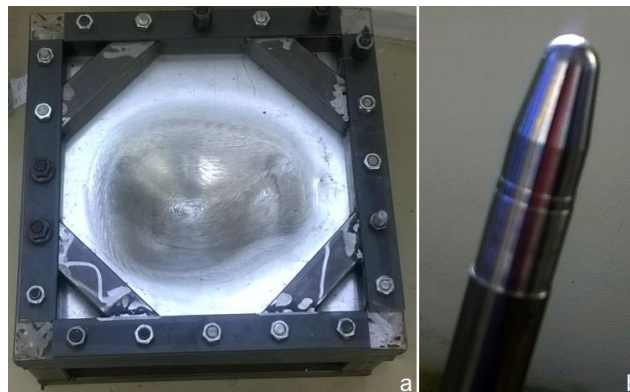

Fig. 6 Equipment used (a) Blank holding fixture with formed sheet (b) SPIF tool

The SPIF process was carried out on an Okuma MX45VAE machining center possessing exceptional rigidity. The spindle motor's maximum power was 14 kW.

6.2. Part quality

The manufactured part is shown in Fig. 7(a). As far as surface quality is concerned, the formation of engravements or 'squeezed out walls' is conspicuous in some places.
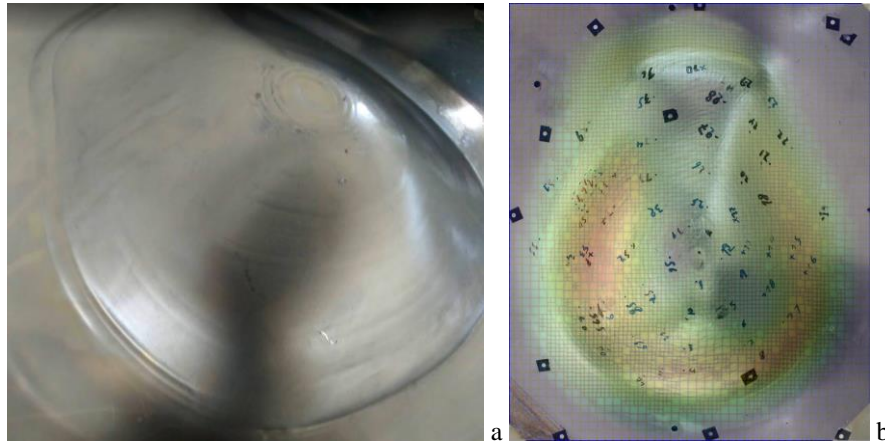
Fig. 7 Manufactured part (a) convex surface (b) overlaid on simulated part of Fig. 3

Shell thickness measurements were taken at 45 points marked on the convex surface of the manufactured part and at the corresponding points of the simulated part (see Fig. 3) as retrieved by Figure overlaying, see Fig. 7(b). Comparison is shown in Fig. 8.
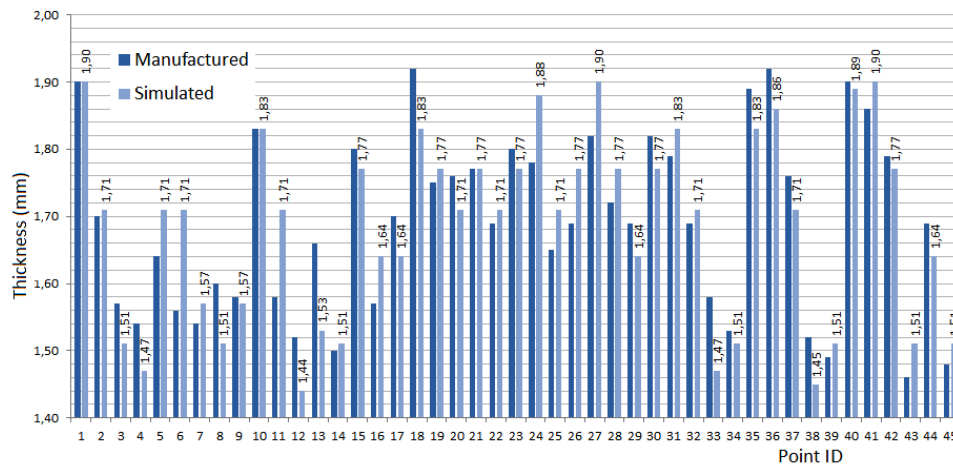
Fig. 8 Shell thickness comparison at 45 points between real and simulated parts

Note that simulated thickness was measured within a range of ±0.033 mm due to FEA postprocessor granularity. Thickness measurements on the manufactured part were taken by a Teledictor 2000™ ultrasonic gauge. The deviation results that are shown in Table 2 exhibit a mean of 0,052 mm and a standard deviation of 0,036 mm, which is practically equal to the accuracy range of simulated thickness measurements. The mean relative deviation between measured and simulated thickness is only 2,22%.

In addition, the manufactured part was digitized using an IMetrics[TM] model ICAM M300 white light scanner and associated software with a nominal accuracy of 70 μm. The concave surface was used as reference for alignment purposes between nominal and real shape. A dimensional comparison of the manufactured part to the simulation prediction on one hand and to the designed nominal shape on the other hand is presented in Fig. 9.
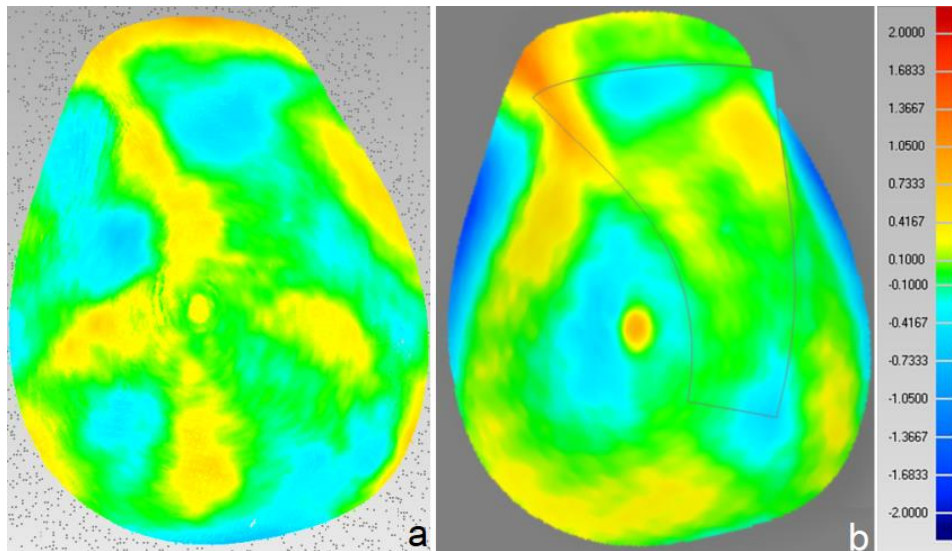
Fig. 9 Part dimensional comparison between real and (a) simulated (b) nominal

In Fig. 9(a) RMS deviation between real and simulated parts is 0.234 mm, whereas according to Fig. 9(b) deviation between real and nominal pats is somewhat larger, i.e. 0.290 mm. Simulation offers good prediction of the final geometry near the "edge" of the cavity, and, in many cases, satisfactory prediction of the deviations in regions with intense curvature, e.g. near vane edge.

Note that final production of the vane requires a metal cutting (finishing) process, typically laser cutting that was not performed in this case.

7. DISCUSSION

Several factors related to the setup of the numerical simulation model may have affected its accuracy. These are briefly discussed next.

Heat dissipation related to friction between the tool and the sheet surface has been neglected in the model; this may change the yield characteristics of the material locally. To some extent, this is overcome by ample use of lubricant, yet its effect has not been quantified. On a related note, spindle speed was not taken into account in modeling either. Finally, the squeezed out wall effect cannot be captured by simulation in the current formulation of mesh discretization and material behavior.

Simplifications have been adopted in the simulation model to alleviate computation load. Regions near the contact and the 'edge' between the cavity bottom and walls have a

substantial curvature compared to shell thickness. Moreover, stress derivative is considerable, especially in the through-thickness direction near the contact. Due to the shell formulation, these aspects of the problem may not be simulated accurately enough. In fact, through-thickness shear force distribution cannot be assessed for validity, although it is comparable to the tensile stress distribution.

Contact stiffness selection affects forces on the contact node. An increased value leads to smaller penetration and increased node speed and its determination was based on experience and experimentation.

According to the boundary conditions employed, the tool is rigid and the sheet is fully clamped on the rigid fixture. This simplification may have a significant impact due to the increased SPIF forces. Indeed, substantial elastic deflections are predicted from supplementary simulations reaching 0.5 mm for the fixture and 0.7 mm for the tool.

Focusing on the impact of element orientation, it is noteworthy that the toolpath is not symmetric with respect to the mesh. Thus, orientation of shell edges in relation to the toolpath varies from 0° to 45°. It is known that Belytchko-Tsay elements are prone to warping [29], especially at increased relative angles between the toolpath and the edges. SPIF of a fully symmetric conical shape was simulated to check such problems, see Fig. 10. Sheet shape representation near the contact with the tool depends on the size of the elements in the direction normal to the toolpath. Stress and strain derivatives as well as curvature are intense there.

Finally, a hypothesis is outlined next, regarding the way in which the shape is deformed away from the contact area, especially in the radial direction and in the presence of substantial curvature.
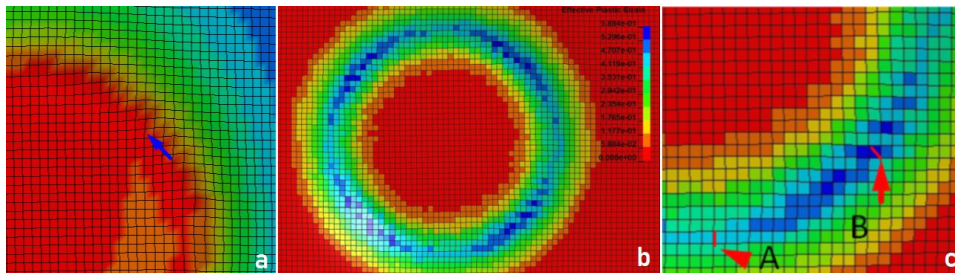
Fig. 10 Impact of finite element orientation in symmetrical part (a) Presence of warping (b) Deviation of plastic strain intensity in the tangential direction (c) Detail of (b)

Referring to Fig. 11(a), 18 nodes are monitored. Displacement along z and x axis is followed for the whole of simulation duration, see Fig. 11(b) and (d).
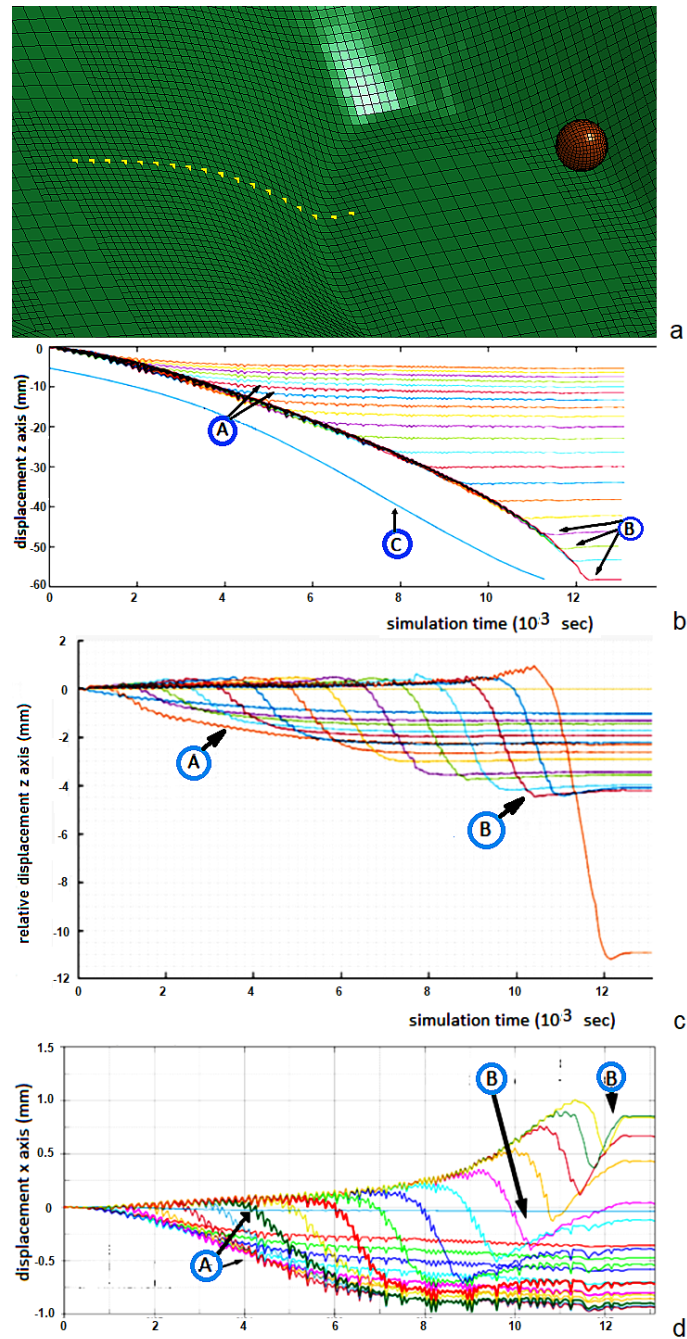
Fig. 11 Node translation (a) Node positions (b) nodes displacement in Z direction   (c) Difference between Z-displacement of adjacent nodes (d) displacement normal to the toolpath (A: nodes close to edges, B: nodes distant from edges C: final cross-section)

Note that in Fig. 11 'A' denotes nodes that are near the edge of the cavity in a convex shape and tend to deform for a longer period, 'B' denotes nodes that are in a convex area and tend to rebound finally ending up with lower final deformation and 'C' denotes the final cross section of the region to which the nodes belong.

When the tool is located at a lower position with respect to a region with high curvature, the tensile stresses caused will lead to deformation and decrease of curvature there. The difference of the displacement (translation) along z-axis between adjacent nodes depicts the resulting deformation, see Fig. 11(c).

Simulation seems to be able to predict this kind of deformation sufficiently. Radial movement of the nodes verifies the hypothesis. An abrupt change in displacement occurs when the tool is in the nodes' region, see Fig. 11(c). Then, nodes in concave regions continue being displaced in the negative direction for a while, whereas nodes in convex regions are displaced in the positive direction.

8. CONCLUSIONS

Usefulness of simulation in planning SPIF for non-symmetric parts has become obvious, as far as the toolpath and process parameter selection is concerned. For the particular choices made in the framework of the case study presented, shape difference between the nominal and real formed parts were predicted to some extent, but what is most important, an insight into the deformation mechanism was gained. Such deviations range within a few tens of a mm (RMS value) which, taking into account the simplifications adopted in numerical modeling of the SPIF process are acceptable.

Simulation duration on a normal personal computer, taking several days, despite the explicit solver being used and the simplifications in modeling, is considered high. It is certainly prohibitive, if a number of alternative scenarios need to be studied, but it can be manageably reduced if high-end computers, GPU / parallel programming techniques are used. The main difficulty stems from the sheer length of the toolpath to be simulated resulting in a very large number of discretized positions of the tool relative to the part.

Future work may follow different directions: (a) Based on the current model (possibly improved through adaptive formulation at the tool contact regions) a systematic study is required so as to determine the optimal way to design the toolpath. (b) Augmentation of the simulation model is desirable, e.g. to incorporate the effect of spindle speed, thermal effects due to friction and lubrication employed, along with a change in constitutive equations of the material due to temperature.

REFERENCES

1. Tera, M., Breaz, R.-E., Racz, S.-G., Girjob, C.-E., 2019, *Processing strategies for single point incremental forming—a CAM approach*, The International Journal of Advanced Manufacturing Technology, 102(5-8), pp. 1761-1777.
2. Jackson, K., Allwood, J., 2009, *The mechanics of incremental sheet forming*, Journal of Materials Processing Technology, 209(3), pp. 1158-1174.
3. Centeno, G., Bagudanch, I., Martínez-Donaire, A.J., García-Romeu, M.L., Vallellano, C., 2014, *Critical analysis of necking and fracture limit strains and forming forces in single-point incremental forming*, Materials & Design, 63, pp. 20-29.
4. Fang, Y., Lu, B., Chen, J., Xu, D.K., Ou, H., 2014, *Analytical and experimental investigations on deformation mechanism and fracture behavior in single point incremental forming*, Journal of Materials Processing Technology, 214(8), pp.1503-1515.
5. Lu, B., Fang, Y., Xu, D. K., Chen, J., Ou, H., Moser, N. H., Cao, J., 2014, *Mechanism investigation of friction-related effects in single point incremental forming using a developed oblique roller-ball tool*, International Journal of Machine Tools and Manufacture, 85, pp. 14-29.
6. Ham, M, Jeswiet, J., 2006, *Single point incremental forming and the forming criteria for AA3003*, CIRP Annals, 55(1), pp. 241-244.
7. Hussain, G., Khan, H.R., Gao, L., Hayat, N., 2013, *Guidelines for tool-size selection for single-point incremental forming of an aerospace alloy*, Materials and Manufacturing Processes, 28(3), pp. 324-329.
8. Hussain, G., Gao, L., Hayat, N., 2011, *Forming parameters and forming defects in incremental forming of an aluminum sheet: Correlation, empirical modeling, and optimization: Part A*, Materials and Manufacturing Processes, 26(12), pp. 1546-1553.
9. Kopac, J., Kampus, Z., 2005, *Incremental sheet metal forming on CNC milling machine-tool*, Journal of Materials Processing Technology, 162-163, pp. 622-628.
10. Skjoedt, M., Bay, N., Endelt, B., Ingarao, G., 2008, *Multi stage strategies for single point incremental forming of a cup*, International Journal of Material Forming, 1, pp. 1199-1202.
11. Blaga, A., Bologa, O., Oleksik, V., Breaz, R. 2011, *Influence of tool path on main strains, thickness reduction and forces in single point incremental forming process*, Proceedings in Manufacturing Systems , 6(4), pp. 2-7.
12. McAnulty, T., Jeswiet, J., Doolan, M., 2017, *Formability in single point incremental forming: A comparative analysis of the state of the art*, CIRP Journal of Manufacturing Science and Technology, 16, pp. 43-54.
13. Lu, B., Chen, J., Ou, H., Cao, J. 2013, *Feature-based tool path generation approach for incremental sheet forming process*, Journal of Materials Processing Technology, 213(7), pp. 1221-1233.
14. 14. Suresh, K., Regalla, S.P., 2014, *Effect of Mesh Parameters in Finite Element Simulation of Single Point Incremental Sheet Forming Process*, Procedia Materials Science, 6, pp. 376-382.
15. Dejardin, S., Thibaud, S., Gelin, J.C., Michel, G., 2010, *Experimental investigations and numerical analysis for improving knowledge of incremental sheet forming process for sheet metal parts*, Journal of Materials Processing Technology, 210(2), pp. 363-369.
16. Naranjo, J., Miguel, V., Martínez-Martínez, A., Gómez-López, L.M., Manjabacas, M.C., Coello, J., 2015, *Analysis and Simulation of Single Point Incremental Forming by ANSYS®*, Procedia Engineering, 132, pp. 1104-1111.
17. Ambrogio, G., Filice, L., Gagliardi, F., Micari, F., 2005, *Sheet Thinning Prediction in Single Point Incremental Forming*, Advanced Materials Research, 6-8, pp. 479-486.
18. ANSYS Inc., 2006, *Thin Wall Structure Simulation*. Ansys Manual.
19. Marinković, D., Rama, G., Zehn, M., 2019, *Abaqus implementation of a corotational piezoelectric 3-node shell element with drilling degree of freedom*, Facta Universitatis Series Mechanical Engineering, 17(2), pp. 269-283.
20. Bambach, M., 2005, *Performance Assessment of Element Formulations and Constitutive Laws for the Simulation of Incremental Sheet Forming (ISF)*, in: O'nate E., Owen D.R.J. (eds.) VIII International Conference on Computational Plasticity 2005, Barcelona, Spain, pp. 1-4.
21. Lequesne, C., Henrard, C., Bouffioux, C., 2008, *Adaptive remeshing for incremental forming simulation*, Numerical Simulation, 32, pp. 4-8.
22. Martínez-Donaire, A.J., Morales-Palma, D., Caballero, A., Borrego, M., Centeno, G., Vallellano, C., 2017, *Numerical explicit analysis of hole flanging by single-stage incremental forming*, Procedia Manufacturing, 13, pp. 132-138.
23. Bouffioux, C., Henrard, C., Gu, J., Duflou, J.R., Habraken, A.M., Sol, H., 2007, *Development of an inverse method for identification of materials parameters in the single point incremental forming process*, in: Tisza, M. (ed.) Proc. Int. Deep Drawing Research Group Conference IDDRG 07, Györ, Hungary, pp. 257-264.
24. Dasappa, P., Inal, K., Mishra, R., 2012, *The effects of anisotropic yield functions and their material parameters on prediction of forming limit diagrams*. International Journal of Solids and Structures,49(25), pp. 3528-3550.

25. ANSYS. 4.2. *Rate-Independent Plasticity*. Ansys 16.2.3.
26. Bouffioux, C., Eyckens, P., Henrard, C., Aerens, R., Van Bael, Q., Sol, H., Duflou, J.R., Habraken, A.M., 2008, *Identification of material parameters to predict Single Point Incremental Forming forces*, International Journal of Material Forming, 1, pp. 1147-1150.
27. Gupta, P., Jeswiet, J., 2019, *Parameters for the FEA simulations of single point incremental forming*, Production and Manufacturing Research, 7(1), pp. 161-177.
28. Hussain, G., Al-Ghamdi, K.A., Khalatbari, H., Iqbal, A., Hashemipour, M., 2014, *Forming parameters and forming defects in incremental forming process: Part B*, Materials and Manufacturing Processes, 29(4), pp. 454-460.
29. Haufe, A., Schweizerhof, K., Dubois, P., 2013, *Properties & Limits : Review of Shell Element Formulations Motivation – from shells to solids*, in: LS-DYNA Developer Forum 2013, Filderstadt, Germany, pp. 1-35.